Supplementary Materials

Simulating contact angle hysteresis using pseudo-line tensions

Ping He, and Chun-Wei Yao

Department of Mechanical Engineering, Lamar University, Beaumont, TX 77710, USA

1. Experimental Setup, Procedures, and Measurements

An experimental setup was built for the sliding-angle experiment, which consisted of a rotation stage system, and image capture system as shown in Fig. S1. The dynamic images of droplets were captured using a high speed camera.

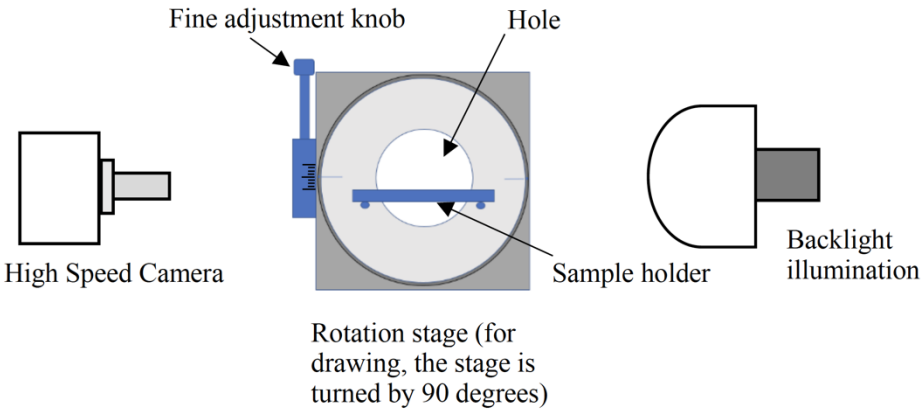

Figure S1. Experimental Apparatus.

2. Numerical Methods

The liquid-air-solid system is modeled as the Newtonian, incompressible multiphase flows governed by the incompressible Navier-Stokes (N-S) equations. The liquid droplet and air are modeled as two continuum regions in the physical domain, while the solid surface is treated as one boundary of the domain. The incompressible multiphase flows are simulated using the volume of fluids (VOF) method. The liquid-air interface is tracked using a VOF function, $0 \le \alpha \le 1$. $\alpha = 1$ marks the liquid region, while $\alpha = 0$ marks the air region. The surface tension force is modeled using the continuum surface force (CSF) model.

A wall level-set function, ϕ_s, is used to represent the solid surface. In general, a level-set function is defined as a signed distance function to identify a specified domain: 1) $|\phi(x,y,z)|$ is the closest distance from (x,y,z) to the domain surface, and 2) ϕ is negative, if (x,y,z) is inside the domain; and ϕ is positive, if outside. A wall delta-function, $\delta_w(\phi)$, is calculated using

$$\delta_w = \begin{cases} \frac{1}{\varepsilon} + \frac{1}{\varepsilon}\cos\left(\frac{\pi\phi_s}{\varepsilon}\right), & \text{if } |\phi| < 2\varepsilon \\ 0 & \text{otherwise} \end{cases} \tag{S-1}$$

where ε is a smearing distance, which is 2× grid size. Note that we only have one side of the solid surface inside the computational domain, i.e. $\phi_s > 0$. The contact line delta function, δ_c, is calculated as

$$\delta_c = |\hat{\boldsymbol{t}} \cdot \nabla\alpha| \tag{S-2}$$

where the tangential direction, $\hat{\boldsymbol{t}}$, of the solid surface, which is normal to the contact line, is calculated as

$$\hat{\boldsymbol{t}} = \frac{\hat{\boldsymbol{n}}_L - (\hat{\boldsymbol{n}}_L \cdot \hat{\boldsymbol{n}})\hat{\boldsymbol{n}}}{|\hat{\boldsymbol{n}}_L - (\hat{\boldsymbol{n}}_L \cdot \hat{\boldsymbol{n}})\hat{\boldsymbol{n}}|} \tag{S-3}$$

$\hat{\boldsymbol{n}}_L = -\nabla\alpha/|\nabla\alpha|$ is the normal direction of the liquid-gas interface pointing towards gas, and $\hat{\boldsymbol{n}} = \nabla\phi_s$ is the unit normal direction of the solid surface pointing towards fluids. The density, ρ, and viscosity, μ, are calculated based on the VOF function, α

$$\rho = \rho_G(1-\alpha) + \rho_L\alpha \tag{S-4}$$

$$\mu = \mu_G(1-\alpha) + \mu_L\alpha \tag{S-5}$$

where the subscript "L" denotes liquid, and "G" gas. The Newtonian stress tensor is

$$\boldsymbol{\tau} = \mu[\nabla\boldsymbol{u} + (\nabla\boldsymbol{u})^T] \tag{S-6}$$

In our simulations, the equilibrium contact angle, θ_{eq}, will be a constant (or variable) input field, which can represent a homogeneous (or heterogeneous) solid surface. The dynamic contact angle, θ, is calculated

$$\cos(\theta) = \hat{\boldsymbol{n}}_L \cdot \hat{\boldsymbol{n}} \tag{S-7}$$

Based on the above equations, the proposed slip boundary condition will be solved explicitly near the contact line (the region of $\delta_c > 0$ and $\delta_w > 0$). The solution, u_s, near the contact line, together with the no-slip condition away from the contact line will be used as the Dirichlet boundary condition of the velocity field in solving the N-S and continuum equations.

3. Simulation Configurations

A water droplet of different sizes (4, 10, 20, and 30 μL) is studied in a 3-D simulation box of 10 mm × 8 mm × 10 mm. A uniform grid size, 0.1 mm, is used for all directions, and a local refinement on the bottom side of the simulation box ($0 \le z \le 3$ mm), where the local grid size is 0.05 mm. The entire domain has 2.48 million cells, and is decomposed into 288 parallel processors. The time step is 0.05 ms, which yields a Courant number less than 0.1. The computation takes about 0.5 second in real time in every 1 ms of the simulated time. Time stepping and grid-size convergence have been studied. Although our code uses 2nd order mixed finite volume/difference schemes, it yields a 1st order the spatial convergence. It may be caused by the VOF and CSF methods used to handle the multiphase flow. The time marching yields a 1st convergence, which is consistent with the Euler method used in our code.

The water droplet is initially deposited on the horizontal substrate in a perfect, partial sphere with the contact angle the same as the experimental value. It is then pulled down by gravity, and after the oscillation stops, the horizontal substrate is gradually inclined to the angle, which is measured in the experiments. Different adhesion tensions are tested to match the following experimental observations simultaneously: (1) the droplet contour, (2) advancing and receding contact angle, and (3) critical condition that the droplet tends to slide. Thus, the adhesion tensions calculated here can be considered as the correct values for a liquid-substrate pair. We find that the advancing and receding sides have different adhesion tensions.

4. Results of a droplet on horizontal PTFE plates

When placing a water droplet on a horizontal flat plate of PTFE as shown in Fig. S2, the droplet forms a spherical shape, if the Bond number ($Bo = \rho g D^2/\sigma$) is small ($Bo < 1$); and with *Bo* increasing over 1, the droplet is flattened by gravity.

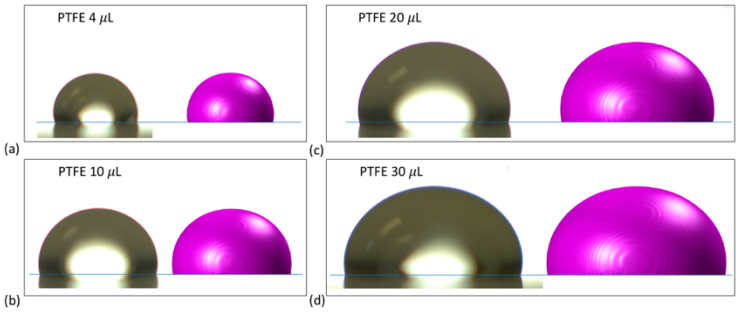

Figure S2. The experimental and simulation contours of a water droplet on a horizontal PTFE plate with the droplet size: (a) 4 μL (*Bo*=0.53), (b) 10 μL (*Bo*=0.97), (c) 20 μL (*Bo*=1.54), and (d) 30 μL (*Bo*=2.03). In each subfigure, the experimental image is on the left, and simulation results on the right.

5. Advancing and receding stresses

Based on our experimental measurements of the Young's, advancing and receding angles at 4 droplet sizes, the advancing and receding stresses, $\left(\gamma_{\mathrm{SLV}}\kappa_{\mathrm{gs}}\right)_{\mathrm{a}}$ and $\left(\gamma_{\mathrm{SLV}}\kappa_{\mathrm{gs}}\right)_{\mathrm{r}}$, are computed using Eq. (10) and shown in Fig. S3. Using the same equation, the advancing and receding stresses of the same water/air/PTFE system computed from Good and Koo's experiments[7] are also shown in Fig. S3. The two sets of experimental data are close but not the same, because different methods have been used: (1) Good and Koo[7] used the sessile drop method, and (2) we use the tilted plate method. The two methods are expected to yield different results.[1] Although both have different advantages and disadvantages, the tilted plate method is selected here, because it is recognized as an excellent method to distinguish the high and low hysteresis.[13]

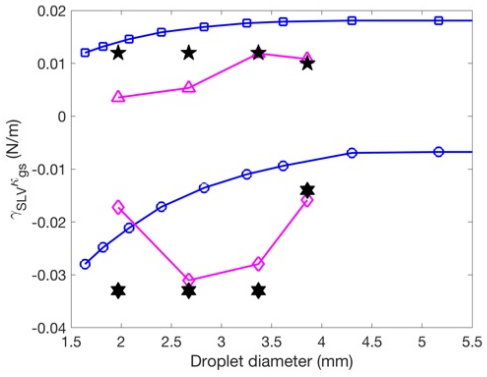

Figure S3. The advancing stress, $\left(\gamma_{SLV}\kappa_{gs}\right)_a$, and receding stress, $\left(\gamma_{SLV}\kappa_{gs}\right)_r$, in the water/air/PTFE system: (1) values computed using Eq. (10) from the data in Good and Koo's experiments,[7] advancing (squares) and receding (circles),

(2) values computed from experiments in this study, advancing (triangles) and receding (diamonds); and (3) simulation values, advancing (pentagrams) and receding (hexagrams).

6. Results of a 20 μL droplet on a tilted PTFE plate

Fig. S4 shows an enlarged view of the droplet image with three simulation contours, which vividly depicts how the advancing and receding stresses affect the droplet contour: A large receding stress will elongate the droplet, while a large advancing stress will thicken the droplet height vertical to the plate. A small change of either or both the advancing and receding stresses will alter the droplet contour and deviate it from the experimental shape.

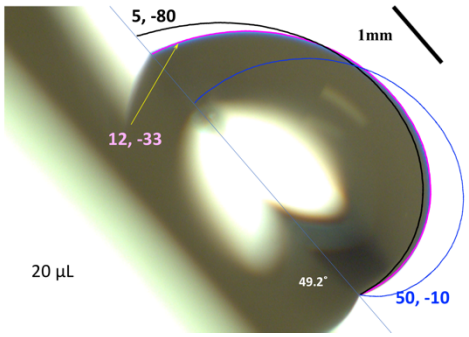

Figure S4. An enlarged view of the 20 μL water droplet on the 49.2° tilted PTFE plate. The simulation contours are plotted overlapped with the experimental image.

7. Results of a 30 μL droplet on a tilted PTFE plate

A 30 μL droplet has a much smaller critical roll-off angle than the 20 μL droplet presented in the previous subsection, because the droplet weight increases. The average critical roll-off angle is 22.6° for 30 μL, and thus, the experimental case, whose critical roll-off angle is 22.4°, is employed in simulations. Fig. S5 shows the droplet contours of the experiment and simulations of three stress pairs. The unique stress pair for the 30 μL droplet case is $\left(\gamma_{\mathrm{SLV}}\kappa_{\mathrm{gs}}\right)_{\mathrm{a}} = 10$ mN/m and $\left(\gamma_{\mathrm{SLV}}\kappa_{\mathrm{gs}}\right)_{\mathrm{r}} = -14$ mN/m, which matches the experimental contour and critical roll-off angle at the same time. The same trend is observed for the 30 μL droplet as for the 20 μL one, that is a larger receding stress elongates the droplet (See Fig. S5c), and a larger advancing stress thickens its height (See Fig. S5d). The critical roll-off stress is $\left(\gamma_{\mathrm{SLV}}\kappa_{\mathrm{gs}}\right)_{\mathrm{a}} - \left(\gamma_{\mathrm{SLV}}\kappa_{\mathrm{gs}}\right)_{\mathrm{r}} < 24$ mN/m, which is less than a half of that in the 20 μL case. The critical roll-off stress is possibly proportional to the lateral component of the droplet weight parallel to the plate. If we assume so, that is

$$\left(\gamma_{\mathrm{SLV}}\kappa_{\mathrm{gs}}\right)_{\mathrm{a}} - \left(\gamma_{\mathrm{SLV}}\kappa_{\mathrm{gs}}\right)_{\mathrm{r}} \propto mg\sin\theta_{cr} \tag{8}$$

where $m = \rho V$ is the droplet mass, $g = 9.81$ m/s^2, θ_{cr} the critical roll-off angle, and V the droplet volume. Since g and ρ are constant, we have $\left(\gamma_{SLV}\kappa_{gs}\right)_{a} - \left(\gamma_{SLV}\kappa_{gs}\right)_{\mathrm{r}} \propto V\sin\theta_{cr}$. For the 20 μL case, $V\sin\theta_{cr} = 15.1$ μL; and for the 30 μL case, $V\sin\theta_{cr} = 11.4$ μL. The deviation of the two cases is slightly above 30%, which is not small but reasonable, because the assumption of Eq. (8) is a simple addition of the advancing and receding stresses, while in reality, the advancing or receding stress, which is the transient stress, σ_{ts}, defined in the subsection of ***defining static pseudo-line tensions for CAH***, varies along the contact line. The line integration of σ_{ts} along the contact line will be the actual value proportional to $V\sin\theta_{cr}$.

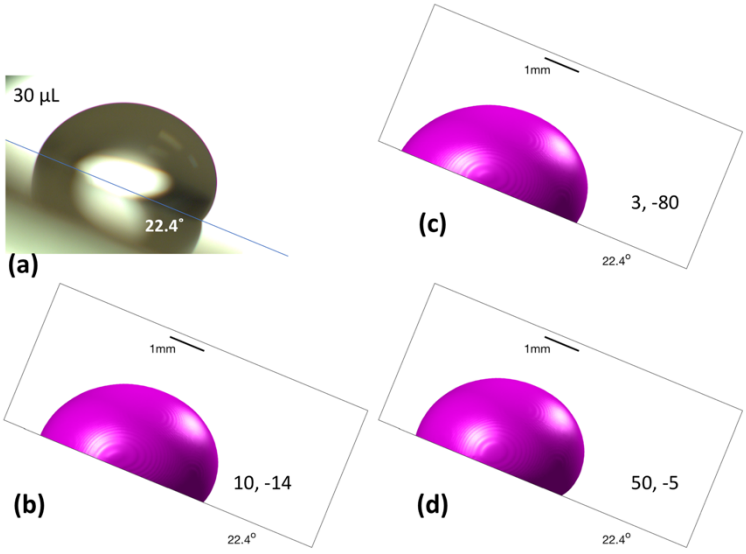

Figure S5. A 30 µL water droplet on a 22.4° tilted PTFE plate immediately before the roll-off event: (a) the experimental image, (b) a simulation with $\left(\gamma_{SLV}\kappa_{gs}\right)_a = 10$ mN/m, and $\left(\gamma_{SLV}\kappa_{gs}\right)_r = -14$ mN/m, (c) $\left(\gamma_{SLV}\kappa_{gs}\right)_a = 3$ mN/m, and $\left(\gamma_{SLV}\kappa_{gs}\right)_r = -80$ mN/m, and (d) $\left(\gamma_{SLV}\kappa_{gs}\right)_a = 50$ mN/m, and $\left(\gamma_{SLV}\kappa_{gs}\right)_r = -5$ mN/m.

Fig. S6 shows an enlarged view of the experimental image of the 30 µL droplet with simulation contours of 4 stress pairs, i.e., (10 mN/m, -14 mN/m), (14 mN/m, -10 mN/m), (3 mN/m, -80 mN/m), and (50 mN/m, -5 mN/m). Although (14 mN/m, -10 mN/m) is not far from to the correct stress pair, its contour plotted in red clearly deviates from the experimental shape. Fig. S7 presents the three-dimensional view of the droplet contours at (10 mN/m, -14 mN/m), (3 mN/m, -80 mN/m), and (50 mN/m, -5 mN/m), and their top view of the contact lines.

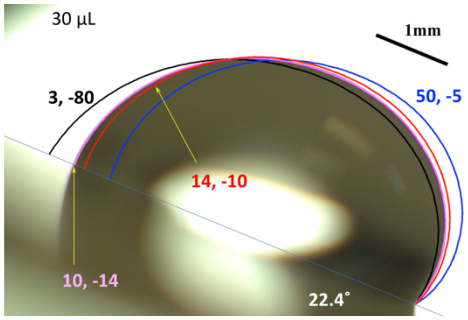

Figure S6. An enlarged view of the 30 µL water droplet on the 22.4° tilted PTFE plate. The simulation contours are plotted overlapped with the experimental image.

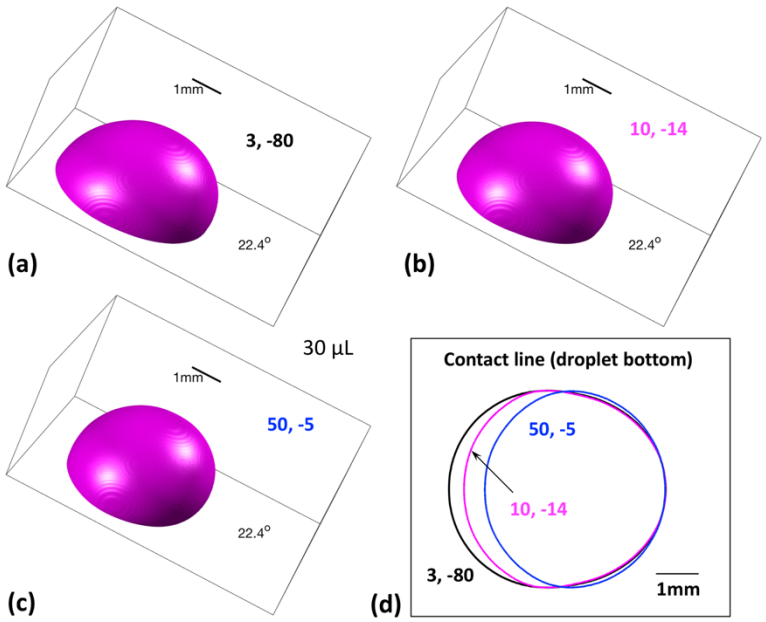

Figure S7. The three-dimensional view of the 30 μL droplets on the 22.4° tilted PTFE plate: (a) $\left(\gamma_{SLV}\kappa_{gs}\right)_a = 3$ mN/m and $\left(\gamma_{SLV}\kappa_{gs}\right)_r = -80$ mN/m, (b) $\left(\gamma_{SLV}\kappa_{gs}\right)_a = 10$ mN/m and $\left(\gamma_{SLV}\kappa_{gs}\right)_r = -14$ mN/m, (c) $\left(\gamma_{SLV}\kappa_{gs}\right)_a = 50$ mN/m and $\left(\gamma_{SLV}\kappa_{gs}\right)_r = -5$ mN/m; and (d) the top view of the droplet/plate contact lines in (a-c).

8. Equilibrium, advancing and receding contact angles for water on PTFE

The experimental and simulation results of contact angles are presented in Fig. S8. Error bars are shown for experimental data, while our simulations do not have an obvious error, since the continuum model itself is a deterministic system. The simulation results agree well with the experiments, and most numerical contact angles fall into the experimental ranges, except for the advancing contact angle in the 20 μL case, whose value is just slightly below the lower bound.

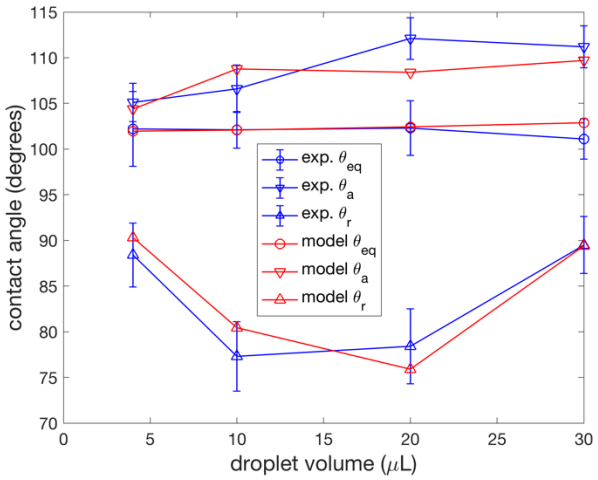

Figure S8. Equilibrium (circle), advancing (down-pointing triangle) and receding (up-pointing triangle) contact angles measured in experiments (blue) and predicted in simulations (red) for water on PTFE. Error bars are shown for experimental data.

9. Results of a water droplet on a copper substrate

In this section, we present the results of a water droplet sitting on a copper substrate, which are similar to those on the PTFE substrate presented in the main text of this letter. Fig. S9 shows a water droplet of different sizes sitting on a horizontal copper substrate, and Fig. S10 shows the same droplet on an inclined copper substrate. Because the 4 and 10 μL cases have not reached the critical sliding condition, any pseudo-line stresses greater than the extreme values will work for the 4 and 10 μL cases. Thus, the pseudo-line stresses in the 4, 10 and 20 μL cases are $\left(\gamma_{SLV}\kappa_{gs}\right)_a = 8$ mN/m and $\left(\gamma_{SLV}\kappa_{gs}\right)_r = -58$ mN/m. The pseudo-line stresses in the 30 μL case are $\left(\gamma_{SLV}\kappa_{gs}\right)_a = 15$ mN/m and $\left(\gamma_{SLV}\kappa_{gs}\right)_r = -60$ mN/m.

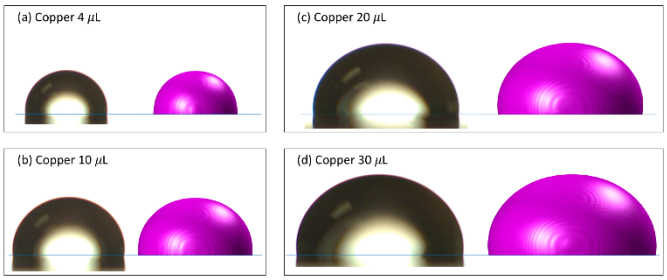

Figure S9. The experimental and simulation contours of a water droplet on a horizontal copper plane with the droplet size: (a) 4 μL, (b) 10 μL, (c) 20 μL, and (d) 30 μL. In each subfigure, the experimental image is on the left, and simulation results on the right.

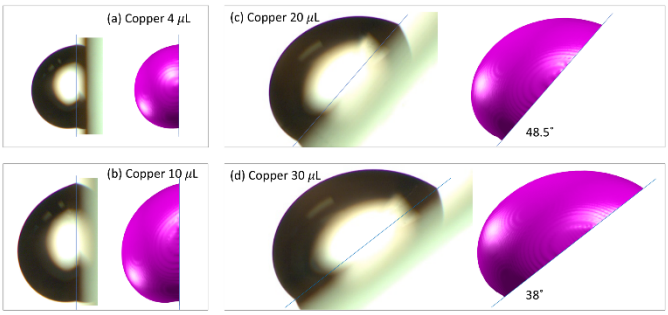

Figure S10. The experimental and simulation contours of a water droplet on an inclined copper plane with the droplet size: (a) 4 μL on a vertical plane, (b) 10 μL on a vertical plane, (c) 20 μL on a 50.9° inclined plane, and (d) 30 μL on a 23.8° inclined plane. In each subfigure, the experimental image is on the left, and simulation results on the right. The sliding condition is not reached in (a) and (b), while the critical sliding condition just occurs in (c) and (d).

Fig. S11 shows the equilibrium, advancing and receding contact angles for water droplets sitting on a horizontal and inclined copper substrate surface, whose experimental and modeling images are shown in Figs. S9 and S10. Good agreement between experimental and simulation results has been observed for equilibrium and receding contact angles.

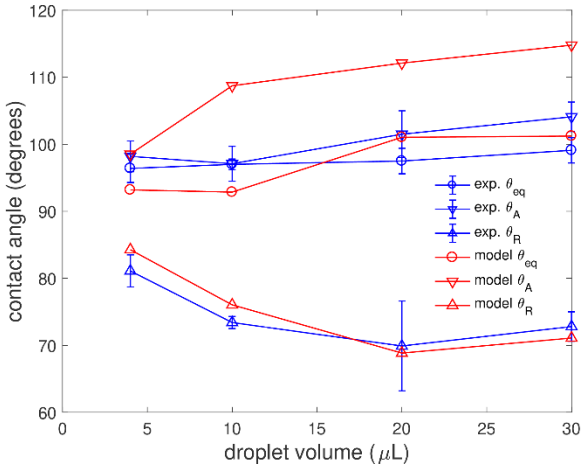

Figure S11. Equilibrium (circle), advancing (down-pointing triangle) and receding (up-pointing triangle) contact angles measured in experiments (blue) and predicted in simulations (red) for water on copper. Error bars are shown for experimental data.